Assembly of the membrane domain of ATP synthase in human mitochondria

Jiuya He[1], Holly C. Ford[1], Joe Carroll, Corsten Douglas, Evvia Gonzales, Shujing Ding, Ian M. Fearnley and John E. Walker[2]

Medical Research Council Mitochondrial Biology Unit, University of Cambridge, Cambridge Biomedical Campus, Hills Road, Cambridge CB2 0XY, United Kingdom

[1] Equal contributions

[2]To whom correspondence should be addressed. e-mail: walker@mrc-mbu.cam.ac.uk

Running title: Assembly of ATP synthase

The authors declare no conflict of interest

Author contributions: J. E. W. designed research and supervised project; J. H., H. C. F., J. C., C. D., E. G., S. D. and I. M. F. performed research; H. C. F., J. H., C. D., J. C., S. D., I. M. F. and J. E. W. analyzed data, and J. E. W. prepared the manuscript.

Classification: BIOLOGICAL SCIENCES, Biochemistry

Key words: human mitochondria; ATP synthase; assembly; membrane subunits

Abstract

The ATP synthase in human mitochondria is a membrane bound assembly of 29 proteins of 18 kinds. All but two membrane components are encoded in nuclear genes, synthesized on cytoplasmic ribosomes and imported into the matrix of the organelle. Here, they are assembled into the complex with ATP6 and ATP8, the products of overlapping genes in mitochondrial DNA. Disruption of individual human genes for the nuclear encoded subunits in the membrane portion of the enzyme leads to the formation of intermediate vestigial ATPase complexes that provide a description of the pathway of assembly of the membrane domain. The key intermediate complex consists of the F_1-c_8 complex inhibited by the ATPase inhibitor protein, IF_1, and attached to the peripheral stalk, with subunits e, f and g associated with the membrane domain of the peripheral stalk. This intermediate provides the template for insertion of ATP6 and ATP8 which are synthesized on mitochondrial ribosomes. Their association with the complex is stabilized by the addition of the 6.8 proteolipid, and the complex is coupled to ATP synthesis at this point. A structure of the dimeric yeast F_o membrane domain is consistent with this model of assembly. The human 6.8 proteolipid (yeast j-subunit) locks ATP6 and ATP8 into the membrane assembly, and the monomeric complexes then dimerize via interactions between ATP6 subunits and between 6.8 proteolipids (j-subunits). The dimers are linked together back-to-face by DAPIT (diabetes associated protein in insulin sensitive tissue; yeast subunit k) forming long oligomers along the edges of the cristae.

Significance Statement

Mitochondria generate the cellular fuel, adenosine triphosphate (ATP) to sustain complex life. Production of ATP depends on oxidation of energy rich compounds to produce the proton motive force (pmf), a chemical potential difference for protons,

across the inner membrane. The pmf drives the ATP synthase, a molecular machine with a rotary action, to synthesize ATP. We have shown that the assembly of human ATP synthase in the inner organellar membrane involves the formation of a monomeric intermediate made from twenty-five nuclear encoded proteins into which the two mitochondrially encoded subunits are inserted and then sealed by association of another nuclear encoded protein, thereby dimerizing the complex. Association of a final nuclear protein oligomerizes the dimers back-to-face along the cristae edges.

Introduction

The ATP synthase in human mitochondria provides most cellular ATP under aerobic conditions. Energy derived from oxidative metabolism generates a proton-motive force (pmf) across the inner membrane of the organelle, and the ATP synthase harnesses the pmf to make ATP from ADP and phosphate (1, 2). Human ATP synthase is an assembly of 29 subunits of 18 types (including the regulatory protein, IF_1) with a combined molecular weight of 592 kDa (3). The subunits are organized into membrane extrinsic and membrane intrinsic domains, linked by central and peripheral stalks (Fig. 1).

The protein subunits emanate from two genomes. In humans and other vertebrates, ATP6 and ATP8 are encoded in overlapping genes in mitochondrial DNA (4) and are translated inside mitochondria. The other subunits, produced from nuclear genes, are translated in the cellular cytoplasm, imported into the organelle and assembled together with ATP6 and ATP8 to produce the complete ATP synthase. Although the assembly of the yeast ATP synthase has been studied extensively (5, 6), until recently, relatively little was known about how human ATP synthase is assembled. However, gene-editing now permits individual subunits of the human enzyme to be removed, and the consequences for assembly can then be examined. Thus, in the absence of subunit c an incomplete ATP synthase is formed lacking the c_8-ring, ATP6,

ATP8, DAPIT and 6.8PL (7). Likewise, removal of either the OSCP or subunit b leads to loss of the entire peripheral stalk, plus ATP6, ATP8, and the five supernumerary subunits, leaving F_1-c_8 inhibited by IF_1 (8). The mitochondria in human ρ^0 cells lack organellar DNA, and contain another incomplete ATP synthase, necessarily with no ATP6 or ATP8 (7, 9). These incomplete vestigial ATP synthases give insights into the pathway of assembly of the complete enzyme. Here, we have investigated the effects of the selective removal of supernumerary membrane subunits e, f, g, DAPIT and 6.8PL on assembly of human ATP synthase.

Results

Human Cells Lacking Supernumerary Subunits. The human genes *ATP5I*, *ATP5J2*, *ATP5L*, *USMG5* and *C14orf2* (*SI Appendix*, Fig. S2) encoding, respectively, subunits e, f, g, DAPIT and 6.8PL of ATP synthase were disrupted in HAP1-WT (wild-type) cells (*SI Appendix,* Tables S1 and S2; Fig. S3). Each of the mutant cells, HAP1-Δe, -Δf, -Δg, -ΔDAPIT and -Δ6.8PL, did not express the eponymous subunit (Fig. 2). The removal of subunits e, f, g or DAPIT had little effect on cellular growth (*SI Appendix*, Fig. S4), except that HAP1-Δe cells reached a similar level of confluence to HAP1-WT cells, and then declined. Also, the growth of HAP1-Δg cells was slightly retarded, but reached a maximum growth similar to controls. In contrast, the removal of 6.8PL retarded cellular growth, but there is no extant explanation. The removal of any one of subunits e, f or g had a severe effect on respiration (*SI Appendix*, Fig. S4), and is similar to removing the OSCP or subunit b or c (7, 8). In HAP1-Δe, -Δf or -Δg cells, the lack of effect of oligomycin indicated that the vestigial ATP synthase is uncoupled from pmf. In HAP1-Δ6.8PL cells, there was evidence of coupled ATP synthase, albeit at reduced levels, and also of a residual functional respiratory chain. The HAP1-ΔDAPIT

cells retained almost normal levels of coupled ATP synthase and respiration. The effects of removal of 6.8PL and DAPIT differ from earlier proposals (10, 11).

Vestigial ATP Synthases. HAP1 cells lacking any one of subunits e, f, g, DAPIT and 6.8PL all assemble vestigial ATP synthase complexes (Fig. 3). Each has a full complement of the α-, β-, γ-, δ- and ε-subunits forming the F_1-domain, and of the peripheral stalk subunits OSCP, b, d and F_6. The HAP1-Δe, -Δf and -Δg cells, but not the HAP1-ΔDAPIT and -Δ6.8PL cells, also lack ATP6 and ATP8. The effects of deleting one supernumerary subunit on the absence or presence of another are more difficult to discern, but removal of either subunit e or g is accompanied by the loss of all other supernumerary subunits, and loss of the 6.8PL accompanies the removal of subunit f.

The subunit compositions of purified vestigial complexes defined by quantitative mass spectrometry (MS) were in agreement with the gel profiles (Fig. 4; *SI Appendix*, Fig. S5; Datasets S1-S10), and the analyses of mitoplasts (*SI Appendix*, Figs. S5 and S6; Datasets S11-S20) were consistent with the following conclusions. Removal of subunit e or g was accompanied by loss of all other supernumerary subunits, plus ATP6 and ATP8. The peripheral stalk subunits were depleted partially, but the rest of the complex was unaffected. The vestigial complex from HAP1-Δf cells lacked ATP6, ATP8, DAPIT and 6.8PL, but otherwise had a full complement of subunits. In contrast, when DAPIT was removed, all other subunits were retained fully. The removal of the 6.8PL led to partial loss of ATP6, ATP8 and DAPIT only. In every instance save one, the formation of the vestigial complexes was accompanied by an elevation in the relative level of IF_1-M1 (7). The exception was the removal of DAPIT where the levels of all forms of IF_1 were unchanged. In mitoplasts from HAP1-Δe, -Δf, -Δg and -Δ6.8PL cells, the relative levels of DAPIT were decreased to a lesser extent

than in vestigial complexes, indicating the presence of the free protein unassociated with the vestigial ATPase complex (*SI Appendix*, Fig. S5). Conversely, the similarities of changes in the content of other subunits between mitoplasts and vestigial ATP synthase complexes, suggests that there is no significant pool of unassembled forms of these subunits.

Oligomeric State of Vestigial ATP Synthases. The oligomeric states of the WT and vestigial ATP synthases became less stable with increasing concentration of digitonin (Fig. 5). There was no evidence for the persistence in any of the mutant cells either of the oligomeric complexes observed in the WT-enzyme, or, with the exception of HAP1-ΔDAPIT cells (Fig. 5; *SI Appendix*, Fig. S7), and possibly -Δf cells (Fig. 5*A*, left panel) of the dimeric complex; the dimeric state in HAP1-ΔDAPIT cells was reduced relative to WT-cells. In contrast, in all cases, a vestigial monomeric complex was present, although in HAP1-Δe, -Δf and -Δg cells, but not in HAP1-Δ6.8PL and HAP1-ΔDAPIT cells, its apparent molecular weight is slightly smaller than that of the monomeric WT-ATP synthase, reflecting their subunit compositions. In HAP1-Δe, -Δf, -Δg and -Δ6.8PL cells, a complex smaller than the monomeric complexes is probably F_1-c_8 (s1 in Fig. 5). In HAP1-WT, -Δf, -ΔDAPIT and -Δ6.8PL, but not -Δe or -Δg cells, there were high levels of a series of smaller sub-complexes (s2 in Fig. 5) containing subunit b, but not F_1-subunits or subunit d.

Turnover of Subunits. When HAP1, HEK or fibroblast cells were grown in the presence of glucose, where the cells are predominantly glycolytic, DAPIT was significantly less stable than any of the other subunits of the ATP synthase including 6.8PL (*SI Appendix*, Fig. S8; Datasets S21-S24). In contrast, when the cells were grown in the presence of galactose, which enforces dependence on oxidative phosphorylation, the difference between DAPIT and other subunits was abolished almost entirely.

Discussion

The vestigial ATP synthase complexes characterized here and previously (7, 8) have been arranged in an order that describes a branched pathway of assembly of the membrane domain of the enzyme (Fig. 6). In one arm, the F_1-c_8 complex, A, is converted to B by addition of the peripheral stalk. Insertion of subunits e and g into B, together or singly in either order, produces complex C, and subsequent addition of subunit f yields complex E. In the second arm, complex D, consisting of the F_1-domain plus the peripheral stalk and subunits e, f and g, is converted to E by the addition of the c_8-ring. In complexes A-E, ATP synthesis is uncoupled from pmf, and the hydrolytic activity of their F_1-domains appears to be inhibited by IF_1. The two arms converge at E, a complex of thirteen nuclear encoded subunits plus IF_1 each imported individually into the mitochondrial matrix before or during assembly. This complex, made of a total of twenty-five proteins, provides the template for the insertion of ATP6 and ATP8 singly, in either order, or together. Both are translated on mitochondrial ribosomes, probably close to the matrix surface of the inner membrane. The resulting complex F is partially coupled to ATP synthesis (*SI Appendix,* Fig. S4*E*), and is somewhat unstable as ATP6 and ATP8 are sub-stoichiometric. The addition of 6.8PL stabilizes ATP6 and ATP8 in complex G, producing an active enzyme coupled to ATP synthesis with no accompanying increase of IF_1 (Fig. 4; *SI Appendix,* Fig. S4*D*).

In mitochondrial membranes, the ATP synthase is dimerized via interactions in the membrane domain, and the dimers form extensive front-to-back rows along the edges of the cristae (12–14). Dimerization of the yeast enzyme depends on the presence of subunits e and g (15), and they associate sequentially with a monomeric complex leading to an assembly ready to dimerize (16). In a structure of the dimeric F_o membrane domain of the yeast enzyme (17), neither of these subunits makes contacts

across the monomer-monomer interface, which involves mainly contacts between the two subunits j and the two ATP6 subunits. However, the requirement for the presence of e and g for dimerization to occur is explained by the assembly pathway for the human enzyme, as both subunits have to be present in the growing complex before ATP6 (and ATP8) can be inserted, and subsequently stabilized by the association of 6.8PL (Fig. 6). Two important conclusions can now be drawn. First, the 6.8PL and yeast subunit j are almost certainly functional orthologs, and relationships between their sequence and positions of trans-membrane α-helices support this view (*SI Appendix,* Fig. S9*A*). Second, dimerization most likely follows the insertion of ATP6 and ATP8 and association of the 6.8 PL. The native gel analyses (Fig. 5) and those published elsewhere (7, 9) are in accord with this suggestion. The final step in the assembly pathway, the addition of DAPIT, produces the fully assembled enzyme, complex H (Fig. 6). DAPIT is the most peripheral of the membrane subunits, and unless it is stabilized by the addition of exogenous phospholipids, mild detergents other than digitonin remove it from the purified complex (18, 19). The most likely role of DAPIT is to form links between dimers of ATP synthase to produce the rows of dimeric complexes along the "edges" of the cristae (12–14). In the model of the yeast dimeric F_o-domain, the incomplete structure of subunit k is associated with subunit ATP6 and is distal from the monomer-monomer interface (Fig. 7). In this position, it is well placed to make contacts between dimers in the oligomeric rows of dimers in mitochondrial inner membranes. It is likely that DAPIT and yeast subunit k are orthologs (*SI Appendix,* Fig. S9*B*). Therefore, the *S. cerevisiae* and human ATP synthases have the same complement of subunits (Table S3). The relative stability of DAPIT under conditions of oxidative metabolism may reflect its role in dimer-dimer interactions

during the re-modeling of mitochondria associated with fission and fusion of the dynamic network of mitochondria in cells.

In *S. cerevisiae*, assembly factors ATP11 and ATP12 participate in the formation of the F_1-domain (20). Another assembly factor FMC1 (formation of complex V assembly factor 1) helps at elevated temperatures, and its loss can be compensated by overexpression of ATP12 (21). The human orthologs are ATPAF1, ATPAF2 and C7orf55 (22, 23), but since their role is in the formation of the F_1-domain, it is unsurprising that they were not significantly associated with complexes A-G (Fig. 6; *SI Appendix*, Fig. S5 and Datasets S1-S20). Another assembly factor INAC (inner membrane assembly complex), made of components of 22 and 17 kDa, is required for the assembly of the yeast peripheral stalk (6, 24). However, no human orthologs have been recognized from sequences, and how the human peripheral stalk is assembled, before being added to the F_1-domain or to complex A (Fig. 6), remains unclear. A subcomplex of subunits b, e and g has been proposed to be an assembly intermediate (25), and it may be among the s2 subcomplexes (Fig. 5*B*). It is worth noting that the extrinsic membrane domain of the bovine peripheral stalk assembles from its four constituent proteins *in vitro*, and that the assembled complex will then associate with the bovine F_1-ATPase spontaneously to produce an F_1-peripheral stalk complex (lacking the membrane domain); both events proceed without the aid of exogenous protein factors (26). The compositions of complexes B and D (Fig. 6) show that the peripheral stalk can be added to either the separate F_1-domain or the F_1-domain in the F_1-c_8 complex, and a similar conclusion has been reached with the yeast ATP synthase (6). The yeast c_{10}-ring probably assembles separate from the F_1-domain or the F_1-peripheral stalk complex, and subsequently the F_1-c_{10} complex or the fully assembled enzyme forms (5, 6). A similar process may operate in human mitochondria, but the

mechanisms of assembly of the c_8-ring and the *S. cerevisiae* c_{10}-ring necessarily differ, as the human c-subunit is encoded by three nuclear genes and is imported into the organelle (27, 28), whereas the yeast c-protein is a mitochondrial gene product made in the mitochondrial matrix (29). Additionally, yeast ATP6 is made as a precursor with an N-terminal extension, which is removed by the inner membrane protease ATP23 during assembly (30, 31); human ATP6 has no precursor. Also, yeast ATP6 and ATP8 are associated first, with either the peripheral stalk or the F_1-peripheral stalk subcomplex, together with assembly factors ATP23, ATP10 and INAC, and then associated with the c_{10}-ring to form the complete complex (5, 6). This pathway differs from the one proposed here for the human enzyme as ATP6 and ATP8 are incorporated after the F_1-peripheral stalk-c_8 complex has formed, and then this complex is stabilized by the 6.8PL (Fig. 6, complexes F and G).

TMEM70 is a membrane protein that has been suggested to participate in the assembly of the membrane domain of human ATP synthase (32, 33), but neither this protein nor any other plausible assembly protein was increased in their association with vestigial complexes A-G (Fig. 6; *SI Appendix*, Fig. S5 and Datasets S1-S20). However, it seems likely that assembly proteins do participate in this pathway, and other methods such as complexomics (34, 35) may be more successful in identifying candidates.

Materials and Methods

Human genes *ATP5I*, *ATP5J2* and *ATP5L* were disrupted in HAP1 cells by CRISPR-Cas9 with pairs of guide RNAs (*SI Appendix*, Table S1) as described before (7), leading to clonal cells HAP1-Δe, -Δf and -Δg, respectively. Clonal cells HAP1-Δ6.8PL (*C14orf2*) and HAP1-ΔDAPIT (*USMG5*) were purchased from Horizon Discovery, Cambridge, U. K. Cell proliferation was monitored with an Incucyte HD instrument

(Essen Bioscience), and the oxygen consumption of cells was measured in a Seahorse XF^{e}24 (Agilent Technologies). The oligomeric state of ATP synthase and vestigial complexes was examined by BN-PAGE and Western blotting. ATP synthase and vestigial complexes were immuno-purified from mitoplasts, analyzed by SDS-PAGE, stained with Coomassie blue and bands analyzed by MS. Proteins were subject to stable isotope labelling by amino acids in cell culture (SILAC), and quantitated by MS. For details, see *SI Appendix*.

Acknowledgements. This work was supported by the Medical Research Council (MRC), U. K. via Programme grant MR/M009858/1 (to J. E. W.). H. C. F. and C. D. received MRC studentships, and E. G., a grant from St John's College, Cambridge. We thank M. G. Montgomery for producing Figs. 1, 6, 7 and S9.

References.

1. Mitchell P (1961) Coupling of phosphorylation to electron and hydrogen transfer by a chemi-osmotic type of mechanism. *Nature* 191:144–148.
2. Walker JE (2013) The ATP synthase: the understood, the uncertain and the unknown. *Biochem Soc Trans* 41:1–16.
3. Walker JE (2017) Chapter 13 Structure, mechanism and regulation of ATP synthases. *Mechanisms of primary energy transduction in biology*, ed Wikström M (The Royal Society of Chemistry, London), pp 338–373.
4. Fearnley IM, Walker JE (1986) Two overlapping genes in bovine mitochondrial DNA encode membrane components of ATP synthase. *EMBO J* 5:2003–2008.
5. Rak M, Gokova S, Tzagoloff A (2011) Modular assembly of yeast mitochondrial ATP synthase. *EMBO J* 30:920–930.
6. Naumenko N, Morgenstern M, Rucktäschel R, Warscheid B, Rehling P (2017) INA complex liaises the F_1F_o-ATP synthase membrane motor modules. *Nat*

Commun 8:1237.

7. He J, et al. (2017) Persistence of the mitochondrial permeability transition in the absence of subunit c of human ATP synthase. *Proc Natl Acad Sci U S A* 114:3409–3414.
8. He J, Carroll J, Ding S, Fearnley IM, Walker JE (2017) Permeability transition in human mitochondria persists in the absence of peripheral stalk subunits of ATP synthase. *Proc Natl Acad Sci U S A* 114:9086–9091.
9. Wittig I, et al. (2010) Assembly and oligomerization of human ATP synthase lacking mitochondrial subunits a and A6L. *Biochim Biophys Acta* 1797:1004–1011.
10. Ohsakaya S, Fujikawa M, Hisabori T, Yoshida M (2011) Knockdown of DAPIT (diabetes-associated protein in insulin-sensitive tissue) results in loss of ATP synthase in mitochondria. *J Biol Chem* 286:20292–20296.
11. Fujikawa M, Ohsakaya S, Sugawara K, Yoshida M (2014) Population of ATP synthase molecules in mitochondria is limited by available 6.8-kDa proteolipid protein (MLQ). *Genes Cells* 19:153–160.
12. Strauss M, Hofhaus G, Schröder RR, Kühlbrandt W (2008) Dimer ribbons of ATP synthase shape the inner mitochondrial membrane. *EMBO J* 27:1154–1160.
13. Dudkina NV, Oostergetel GT, Lewejohann D, Braun HP, Boekema EJ (2010) Row-like organization of ATP synthase in intact mitochondria determined by cryo-electron tomography. *Biochim Biophys Acta* 1797:272–277.
14. Davies KM, et al. (2011) Macromolecular organization of ATP synthase and complex I in whole mitochondria. *Proc Natl Acad Sci U S A* 108:14121–14126.
15. Arnold I, Pfeiffer K, Neupert W, Stuart RA, Schägger H (1998) Yeast mitochondrial F_1F_o-ATP synthase exists as a dimer: identification of three dimer-

specific subunits. *EMBO J* 17:7170–7178.

16. Wagner K, et al. (2009) Mitochondrial F_1F_o-ATP synthase: the small subunits e and g associate with monomeric complexes to trigger dimerization. *J Mol Biol* 392:855–861.
17. Guo H, Bueler SA, Rubinstein JL (2017) Atomic model for the dimeric F_o region of mitochondrial ATP synthase. *Science* 358:936–940.
18. Chen R, Runswick MJ, Carroll J, Fearnley IM, Walker JE (2007) Association of two proteolipids of unknown function with ATP synthase from bovine heart mitochondria. *FEBS Lett* 581:3145–3148.
19. Meyer B, Wittig I, Trifilieff E, Karas M, Schägger H (2007) Identification of two proteins associated with mammalian ATP synthase. *Mol Cell Proteomics* 6:1690–1699.
20. Ackerman SH (2002) Atp11p and Atp12p are chaperones for F_1-ATPase biogenesis in mitochondria. *Biochim Biophys Acta* 1555:101–105.
21. Lefebvre-Legendre L, et al. (2001) Identification of a nuclear gene (*FMC1*) required for the assembly/stability of yeast mitochondrial F_1-ATPase in heat stress conditions. *J Biol Chem* 276:6789–6796.
22. Wang ZG, White PS, Ackerman SH (2001) Atp11p and Atp12p are assembly factors for the F_1-ATPase in human mitochondria. *J Biol Chem* 276:30773–30778.
23. Li Y, Jourdain AA, Calvo SE, Liu JS, Mootha VK (2017) CLIC, a tool for expanding biological pathways based on co-expression across thousands of datasets. *PLoS Comput Biol* 13:e1005653.
24. Lytovchenko O, et al. (2014) The INA complex facilitates assembly of the peripheral stalk of the mitochondrial F_1F_o-ATP synthase. *EMBO J* 33:1624–1638.

25. Fujikawa M, Sugawara K, Tanabe T, Yoshida M (2015) Assembly of human mitochondrial ATP synthase through two separate intermediates, F_1-c-ring and b-e-g complex. *FEBS Lett* 589:2707–2712.

26. Collinson IR, et al. (1994) ATP synthase from bovine heart mitochondria. *In vitro* assembly of a stalk complex in the presence of F_1-ATPase and in its absence. *J Mol Biol* 242:408–421.

27. Dyer MR, Walker JE (1993) Sequences of members of the human gene family for the c subunit of mitochondrial ATP synthase. *Biochem J* 293:51–64.

28. Yan WL, Lerner TJ, Haines JL, Gusella JF (1994) Sequence analysis and mapping of a novel human mitochondrial ATP synthase subunit 9 cDNA (ATP5G3). *Genomics* 24:375–377.

29. Hensgens LA, Grivell LA, Borst P, Bos JL (1979) Nucleotide sequence of the mitochondrial structural gene for subunit 9 of yeast ATPase complex. *Proc Natl Acad Sci U S A* 76:1663–1667.

30. Osman C, Wilmes C, Tatsuta T, Langer T (2007) Prohibitins interact genetically with Atp23, a novel processing peptidase and chaperone for the F_1F_o-ATP synthase. *Mol Biol Cell* 18:627–635.

31. Zeng X, Neupert W, Tzagoloff A (2007) The metalloprotease encoded by ATP23 has a dual function in processing and assembly of subunit 6 of mitochondrial ATPase. *Mol Biol Cell* 18:617–626.

32. Cízková A, et al. (2008) TMEM70 mutations cause isolated ATP synthase deficiency and neonatal mitochondrial encephalocardiomyopathy. *Nat Genet* 40:1288–1290.

33. Vrbacký M, et al. (2016) Knockout of TMEM70 alters biogenesis of ATP synthase and leads to embryonal lethality in mice. *Hum Mol Genet* 25:4674–4685.

34. Heide H, et al. (2012) Complexome profiling identifies TMEM126B as a component of the mitochondrial complex I assembly complex. *Cell Metab* 16:538–549.

35. Guerrero-Castillo S, et al. (2017) The assembly pathway of mitochondrial respiratory chain complex I. *Cell Metab* 25:128–139.

Figure Legends

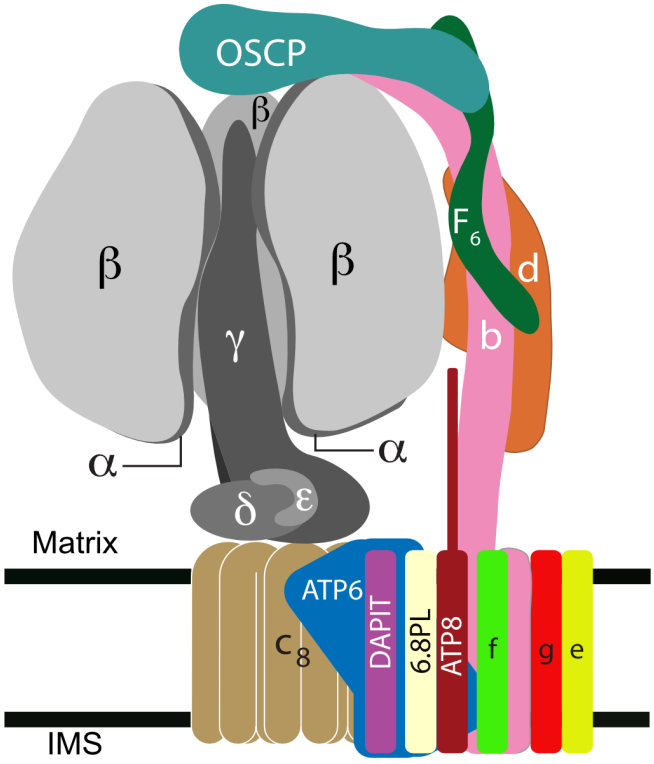

Fig. 1. Organization of subunits in monomeric ATP synthase in mammalian mitochondria. Black horizontal lines represent the inner membrane; IMS, inter-membrane space. The peripheral stalk (subunits OSCP, F_6, b and d) is on the right. Subunit b has two N-terminal transmembrane α-helices interacting directly or indirectly with subunits e, f, g, DAPIT and 6.8PL, which have no known roles in synthesis or hydrolysis of ATP. Each has a single predicted transmembrane α-helix (*SI Appendix*, Fig. S1). The membrane domain of subunit b is associated with mitochondrially

encoded subunits ATP6 and ATP8. The N-terminal region of ATP8 has a single transmembrane α-helix and its C-terminal region extends into the peripheral stalk; ATP8 and subunit b keep ATP6 in contact with the c_8-ring. The pmf drives the rotation of this ring and the attached central stalk (subunits γ, δ and ε) by the translocation of protons through the interface between the c_8-ring and ATP6. The rotation of the central stalk carries energy into the three catalytic sites in the F_1 domain (subunit composition $\alpha_3\beta_3\gamma\delta\varepsilon$); an α-subunit has been removed to expose the central γ-subunit.

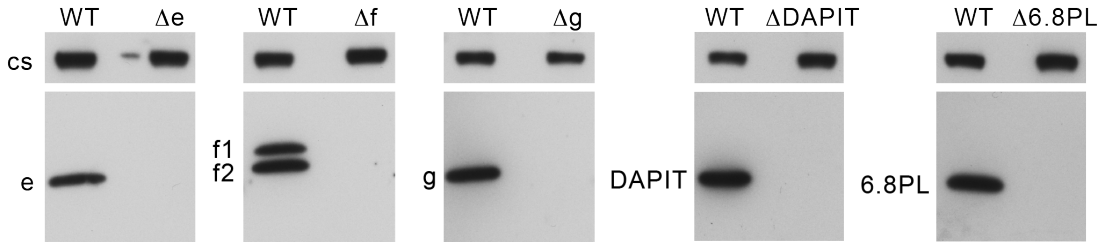

Fig. 2. Absence from clonal HAP1 cells of individual supernumerary subunits of ATP synthase. Mitoplasts were prepared from HAP1-wild type (WT) cells and HAP1-Δe, -Δf, -Δg, -ΔDAPIT and -Δ6.8PL clonal cells. In the HAP1-Δf cells, f1 and f2 denote isoforms of subunit f. The mitoplasts were extracted with dodecylmaltoside. The extracts were fractionated by SDS-PAGE and Western blotted with antibodies against the corresponding subunits. Citrate synthase (cs) provided loading controls.

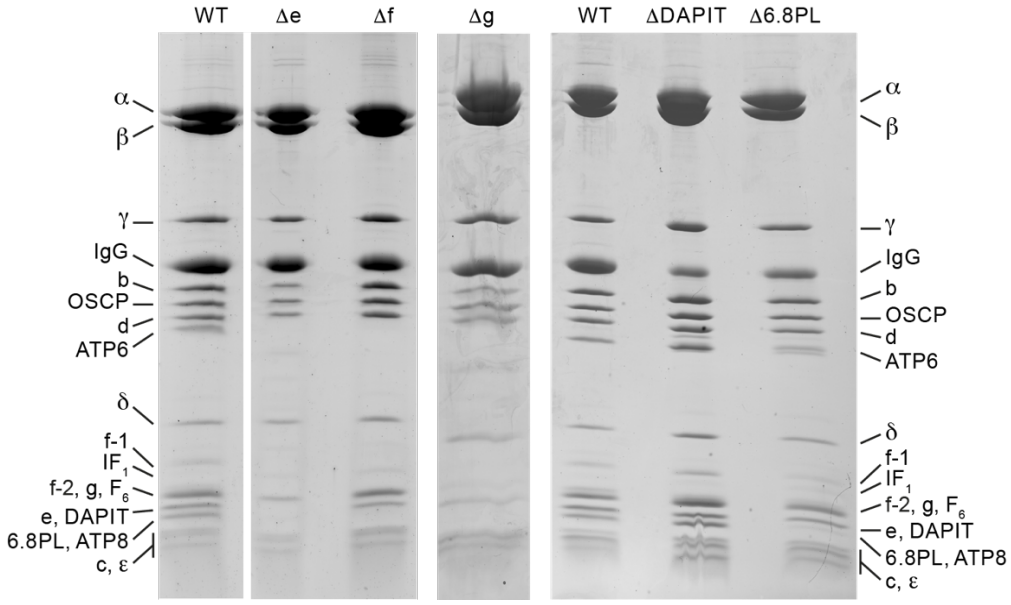

Fig. 3. Subunit compositions of vestigial ATP synthase complexes produced by removal of individual supernumerary membrane subunits. The complexes were immuno-purified from mitoplasts derived from HAP1-WT (wild type), -Δe, -Δf, -Δg, -ΔDAPIT and -Δ6.8PL cells, fractionated by SDS-PAGE and stained with Coomassie blue. The positions of subunits are indicated. IgG, immunoglobulin.

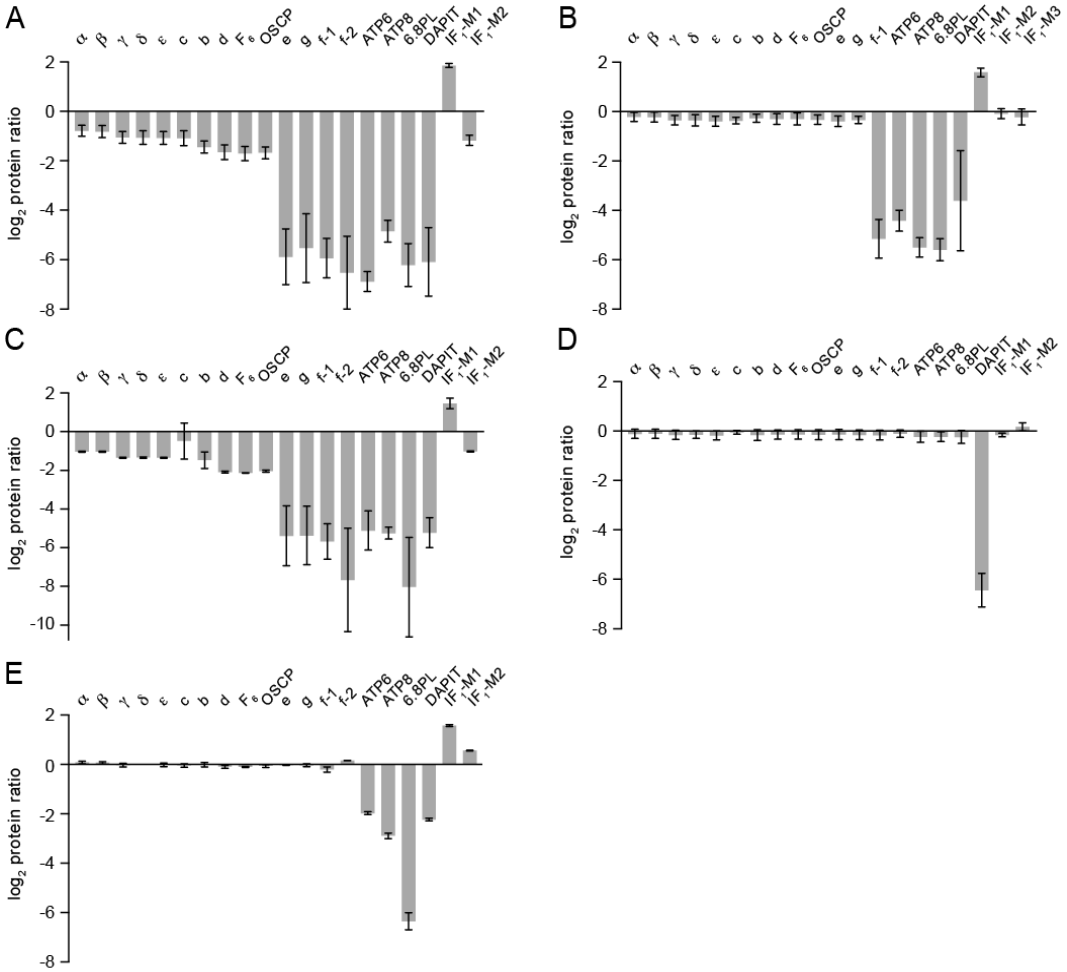

Fig. 4. Effects of removal of individual supernumerary membrane subunits on human ATP synthase. (*A*)-(*E*), relative abundances of subunits, and forms M1, M2 and M3 of IF_1, in immuno-purified ATP synthase and vestigial complexes, from clonal cells. (*A*), HAP1-Δe; (*B*), HAP1-Δf; (*C*), HAP1-Δg; (*D*), HAP1-ΔDAPIT; and (*E*), HAP1-Δ6.8PL. The histograms, derived from *SI Appendix*, Fig. S5 and Datasets S1-S10, are the median values of both relative abundance ratios determined for proteins found in complementary SILAC experiments. Error bars show the range of the two values. IF_1-M1, -M2 and -M3 are different mature forms of IF_1, and f-1 and f-2 are isoforms of subunit f (Swissprot P56134). Similar experiments conducted on mitoplasts are presented in *SI Appendix* Fig. S6.

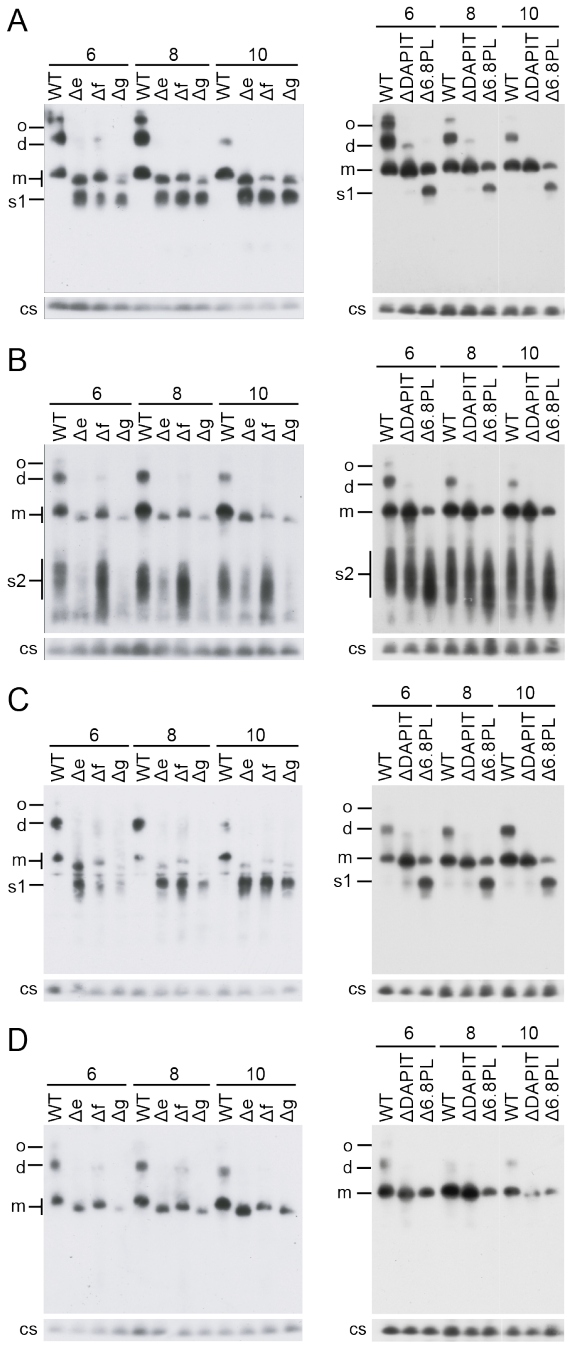

Fig. 5. Oligomeric states of ATP synthase and vestigial forms in HAP1 cells. ATP synthase and vestigial complexes were extracted at various digitonin/protein (g/g) ratios indicated above the lanes, from mitoplasts of HAP1-WT, HAP1-Δe, HAP1-Δf, HAP1-Δg, HAP1-ΔDAPIT, and HAP1-Δ6.8PL cells. Extracts were fractionated by BN-PAGE, and complexes were revealed by Western blotting with antibodies against various subunits of ATP synthase: (*A*), β-subunit; (*B*), b-subunit; (*C*), γ-subunit; (*D*), d-subunit. cs, citrate synthase as loading control. The positions of the complexes are

indicated on the left; o, oligomers; d, dimers; m, monomers; s1, F_1-c_8 sub-complexes; s2, sub-complexes containing subunits b, e and g.

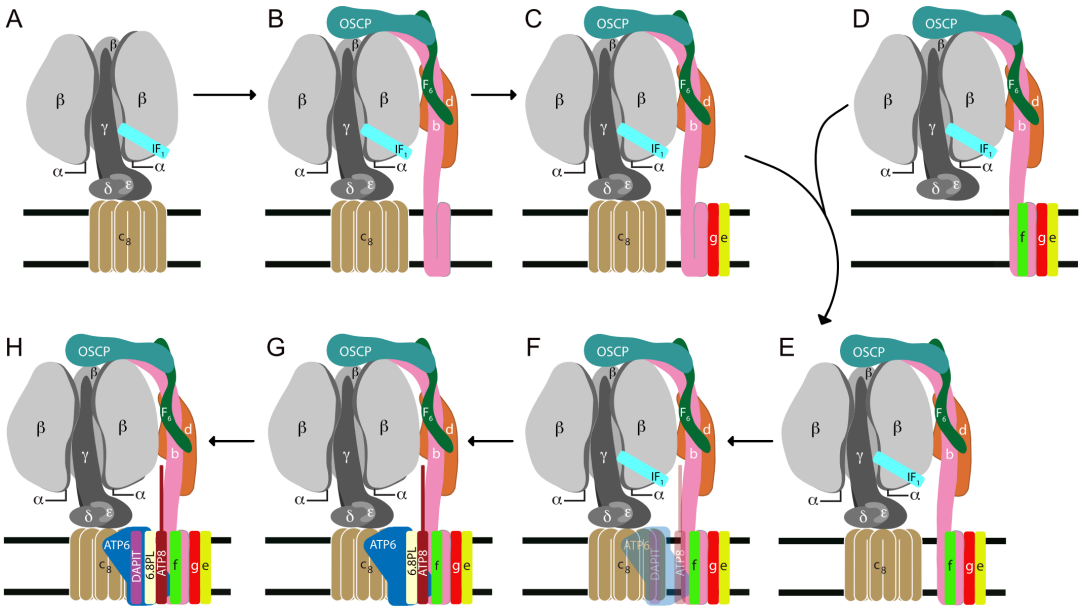

Fig. 6. Pathway of assembly of the membrane domain of human ATP synthase. Panels A-D and F and G, intermediate vestigial complexes, and subunit compositions characterized from mitochondria of clonal cells: A, HAP1-Δb or -ΔOSCP; B, HAP1-Δe or -Δg; C, HAP1-Δf; D, HAP1-Δc; F, HAP1-Δ6.8PL; G, HAP1-ΔDAPIT. E, vestigial complex from the mitochondria of ρ^0 cells. The horizontal black lines denote the boundaries of the inner mitochondrial membrane. Panel H, the complete monomeric ATP synthase.

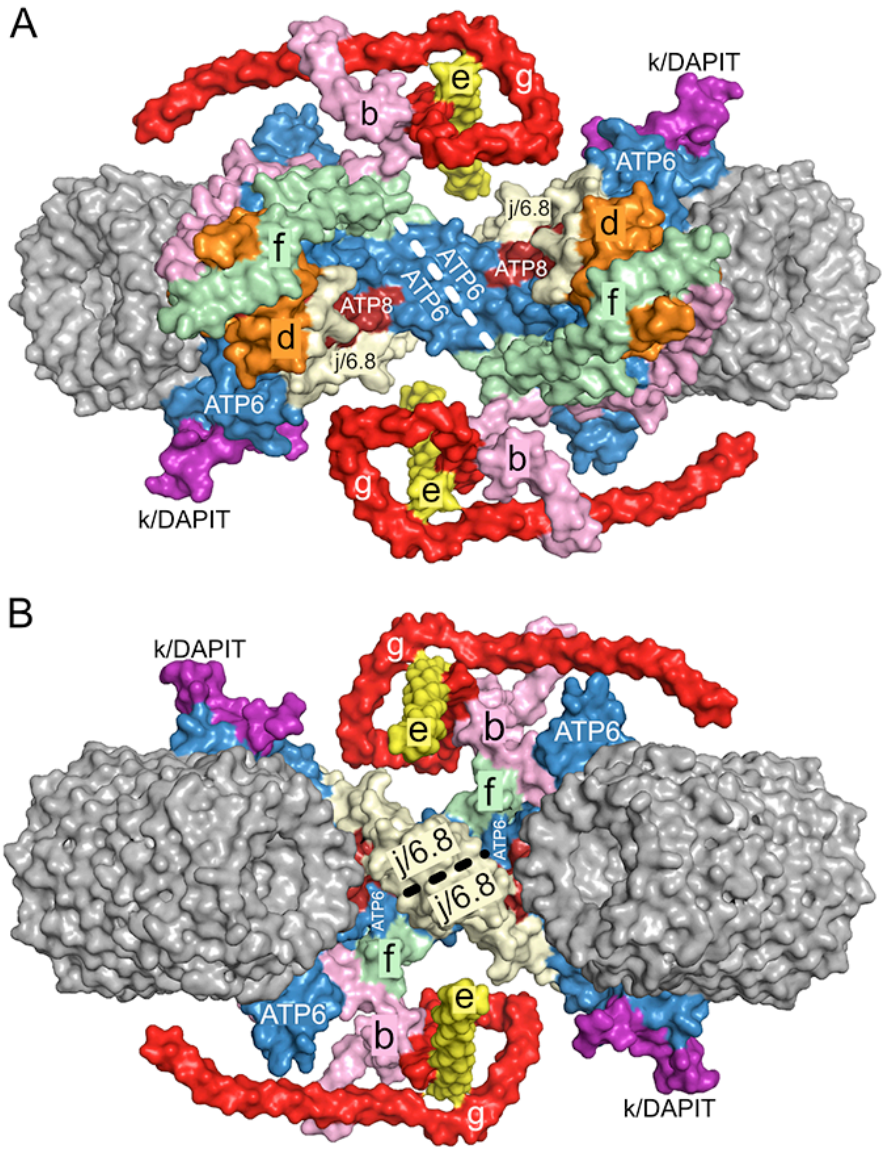

Fig. 7. Structure of the dimeric F_o domain the ATP synthase from *S. cerevisiae* (17). The c_{10}-ring is grey and other subunits are colored and identified on the structures. In (*A*) and (*B*), the two associated monomers are viewed from the matrix and from the inter-membrane space, respectively. The interface between monomers is formed mainly by the two ATP6 (or a) subunits and by the two j-subunits. Here, it is proposed that subunit j and the human 6.8PL (labelled 6.8) are orthologs. It is also proposed that subunit k is the ortholog of human DAPIT and that these subunits assist in the formation of oligomeric structures consisting of rows of dimers along the edges of the mitochondrial cristae.

***SI Appendix* for:**

Assembly of the membrane domain of ATP synthase in human mitochondria

Jiuya He, Holly C. Ford, Joe Carroll, Corsten Douglas, Evvia Gonzales, Shujing Ding, Ian M. Fearnley and John E. Walker

Medical Research Council Mitochondrial Biology Unit, University of Cambridge, Cambridge Biomedical Campus, Hills Road, Cambridge CB2 0XY, United Kingdom

Materials and Methods

Gene disruptions. The genes for the e, f, g, DAPIT and 6.8PL subunits were disrupted individually in human HAP1-WT cells by CRISPR-Cas9 technology (1). The structures of the genes are shown in *SI Appendix*, Fig. S2. HAP1 cells have a haploid karyotype, except for the presence of a fragment of chromosome 15 in chromosome 19 and a reciprocal translocation between chromosomes 9 and 22. None of these features affects the genes in question, as *ATP5I*, *ATP5J2*, *ATP5L, USMG5* and *C14orf2* are on chromosomes 4, 7, 11, 10 and 14, respectively. For *ATP5I*, *ATP5J2* and *ATP5L*, pairs of gRNAs characteristic of exon I and intron A were selected (*SI Appendix*, Table S1). Each pair was introduced independently into HAP1-WT cells, and screening of clones from single cells for the absence of subunit e, f or g led to the identification of HAP1-Δe, -Δf and -Δg cells. The deletions in HAP1-Δe, -Δf and -Δg cells were 51, 83 and 104 bp, respectively, (*SI Appendix*, Table S2 and Fig. S3, parts *A*, *B* and *C*). Each deletion had arisen from two gRNAs and non-homologous end-joining of the deleted genomic DNA. All three deletions included the translational start codon and upstream sequence, and extended across the junction between exon I and intron A, into intron A. The gene disruptions of *USMG5* and

C14orf2 in HAP1-ΔDAPIT and HAP1-Δ6.8PL cells, had been introduced with single gRNA molecules by Horizon Discovery, Cambridge, U. K. The 43 bp deletion in the former extends from the 3' end of intron B into exon III, and does not include the translational start codon, which is in exon II, and the impact on transcription of the 5'-coding region is not known (*SI Appendix*, Fig. S3*D*). The 10 bp deletion in the HAP1-Δ6.8PL cells introduces a frame-shift after codon 17 with the effects of conserving codon 18, mutating codons 19-22 and introducing a termination codon at codon 23 (*SI Appendix*, Fig. S3*E*).

Cell Culture. HAP1-WT (Horizon Discovery) and clonal cells were cultured in Iscove's modified Dulbecco's medium under standard conditions (2). Cell proliferation was monitored with an Incucyte HD instrument (Essen Bioscience) and oxygen consumption rate (OCR) was measured in a Seahorse XF^e24 analyzer (Agilent Technologies), as described before (2). OCR was normalized to cell number by the sulforhodamine B assay (3). Stable isotope labelling of proteins with amino acids in cell culture (SILAC) of HAP1-WT and gene disrupted clonal cells was carried out as described before (2). Human embyonic kidney cells (HEK293) and immortalized human skin fibroblast cells (a gift from Dr. E. Fernandez-Vizarra, MRC-Mitochondrial Biology Unit, Cambridge, U. K.) were cultured at 37°C under 5% CO_2 in high glucose (4.5 g/l) Dulbecco's Modified Eagle Medium (DMEM) supplemented with fetal bovine serum (10% v/v), penicillin (100 U/ml) and streptomycin (100 μg/ml). To assess the effect on protein turnover of substituting glucose for galactose in cell culture media, skin fibroblasts were cultured in DMEM lacking glucose, pyruvate and all amino acids (Dundee Cell Products Ltd, Dundee, U. K.), supplemented for SILAC, and in addition with glucose (25 mM) or galactose (25

mM), pyruvate (1 mM) and all other amino acids at standard concentrations for DMEM.

General methods. Cell protein concentrations were determined by either the bicinchoninic acid assay (Thermo Fisher Scientific) or the detergent compatible protein assay (BioRad). Mitoplasts were prepared from cells with digitonin, as described before (2, 4). Extracts of mitoplasts made with dodecylmaltoside (DDM; 1%, w/v) were fractionated by SDS-PAGE, and subunits of ATP synthase and citrate synthase were detected by Western blotting. The oligomeric states of ATP synthase and vestigial complexes in digitonin extracts of mitoplasts were examined by BN-PAGE and Western blotting. Samples of mitoplasts were re-suspended to *ca.* 5 mg/ml in NativePAGE sample buffer (Thermo Fisher Scientific) containing digitonin (6-10 g/g protein), kept at 4°C for 15 min, and then centrifuged (10,500 x *g*, 20 min, 4°C). The supernatants were treated with benzonase (Merck Millipore) at room temperature, centrifuged again, and soluble complexes fractionated by BN-PAGE at 4°C in 3-12% acrylamide gradient Bis-Tris gels (Thermo Fisher Scientific) according to the manufacturer's instructions for Western blotting. The origins of the antibodies have been described before (5), or are given in *SI Appendix* Table S4. ATP synthase was purified from digitonin solubilized mitoplasts with an immuno-capture resin (Abcam) as described before (2). For the SDS-PAGE profiles (Fig. 3), digitonin in the bead wash solution was replaced by DDM (0.05% w/v). Samples for mass spectrometric analysis were reduced and alkylated in gel sample buffer, fractionated by SDS-PAGE and stained with Coomassie blue R250 dye (6). Bands were excised and proteins digested in-gel with trypsin (7). The extracted peptide mixtures were analyzed in a MALDI-TOF-TOF instrument (model 4800, AB-Sciex) and the proteins were identified from the tandem-MS data (8).

Protein quantitation. Relative quantitation of proteins was derived from mass spectrometric data from SILAC samples (9). LC-MS-MS of tryptic peptide mixtures was performed on a Proxeon EASY-nLC system coupled directly to a Q-Exactive Orbitrap mass spectrometer (Thermo Fisher Scientific). Heavy and light peptide mass data were analyzed with MaxQuant version 1.5.8.3, and the integrated Andromeda search engine (10, 11) employing a Swiss-Prot human protein database (January 2017) modified to include mature forms of ATPIF1, denoted as IF_1-M1, -M2 and -M3, with N-terminal residues Phe-25, Gly-26 and Ser-27, respectively (12, 13). Search parameters were: MS tolerance 4.5 p.p.m.; MS/MS tolerance 20 p.p.m.; Trypsin/P with two missed cleavages; Cys-carbamidomethyl fixed; oxidation (Met) and acetyl (protein N-term) variable; Arg-10 and Lys-8. The MaxQuant output was managed further with Perseus (14). Protein ratios for ATPIF1 were calculated manually using data specific for the unique N-terminal peptides of the various mature forms of ATPIF1, located in the MaxQuant evidence file, and represent the median of the assigned specific peptide ratios, where MaxQuant ISO-MSMS peptide values were used only if fewer than three MULTI-MSMS peptide ratios were obtained. The basis of quantitative experiments using SILAC has been described previously (15).

Analysis of turnover rates of ATP synthase subunits in the native enzyme. Cells were cultured for 24 h in light SILAC medium, transferred into heavy SILAC medium for varying periods of time (1-24 h), washed with PBS and then harvested. Mitochondrial inner membranes were prepared from the cells (6) and membrane protein complexes extracted with DDM (3 g/g protein) and analyzed by BN-PAGE. The proteins in the gels were stained with Coomassie blue R250. Bands corresponding to monomeric ATP synthase were excised and the proteins were digested in-gel with trypsin. The peptides were extracted and relative quantitation of

proteins was performed by quantitative mass spectrometry and MaxQuant data processing as described above. Heavy/light protein ratios were transformed to give the proportion of light labelled protein, and were expressed as the percentage of light labelled protein remaining at each time point. Because the cells proliferate, the quantity of heavy labelled proteins increases over time. Therefore, the absolute rates of protein turnover were not determined, but the values represent the relative differences in equilibrium state established by synthesis and degradation of proteins.

References

1. Ran FA, et al. (2013) Genome engineering using the CRISPR-Cas9 system. *Nat Protoc* 8:2281–2308.
2. He J, et al. (2017) Persistence of the mitochondrial permeability transition in the absence of subunit c of human ATP synthase. *Proc Natl Acad Sci U S A* 114:3409–3414.
3. Skehan P, et al. (1990) New colorimetric cytotoxicity assay for anticancer-drug screening. *J Natl Cancer Inst* 82:1107–1112.
4. Klement P, Nijtmans LG, Van den Bogert C, Houstěk J (1995) Analysis of oxidative phosphorylation complexes in cultured human fibroblasts and amniocytes by blue-native-electrophoresis using mitoplasts isolated with the help of digitonin. *Anal Biochem* 231:218–224.
5. He J, Carroll J, Ding S, Fearnley IM, Walker JE (2017) Permeability transition in human mitochondria persists in the absence of peripheral stalk subunits of ATP synthase. *Proc Natl Acad Sci U S A* 114:9086–9091.
6. Rhein VF, Carroll J, Ding S, Fearnley IM, Walker JE (2013) NDUFAF7 methylates arginine 85 in the NDUFS2 subunit of human complex I. *J Biol Chem* 288:33016–33026.

7. Wilm M, et al. (1996) Femtomole sequencing of proteins from polyacrylamide gels by nano-electrospray mass spectrometry. *Nature* 379:466–469.
8. Rhein VF, et al. (2014) Human METTL20 methylates lysine residues adjacent to the recognition loop of the electron transfer flavoprotein in mitochondria. *J Biol Chem* 289:24640–24651.
9. Ong SE, et al. (2002) Stable isotope labeling by amino acids in cell culture, SILAC, as a simple and accurate approach to expression proteomics. *Mol Cell Proteomics* 1:376–386.
10. Cox J, Mann M (2008) MaxQuant enables high peptide identification rates, individualized p.p.b.-range mass accuracies and proteome-wide protein quantification. *Nat Biotechnol* 26:1367–1372.
11. Cox J, et al. (2011) Andromeda: a peptide search engine integrated into the MaxQuant environment. *J Proteome Res* 10:1794–1805.
12. Xu G, Shin SB, Jaffrey SR (2009) Global profiling of protease cleavage sites by chemoselective labeling of protein N-termini. *Proc Natl Acad Sci U S A* 106:19310–19315.
13. Vaca Jacome AS, et al. (2015) N-terminome analysis of the human mitochondrial proteome. *Proteomics* 15:2519–2524.
14. Tyanova S, et al. (2016) The Perseus computational platform for comprehensive analysis of (prote)omics data. *Nat Methods* 13:731–740.
15. Cox J, Mann M (2011) Quantitative, high-resolution proteomics for data-driven systems biology. *Annu Rev Biochem* 80:273–299.
16. Drozdetskiy A, Cole C, Procter J, Barton GJ (2015) JPred4: a protein secondary structure prediction server. *Nucleic Acids Res* 43:W389–94.
17. Jones DT (1999) Protein secondary structure prediction based on position-

specific scoring matrices. *J Mol Biol* 292:195–202.

18. Krogh A, Larsson B, von Heijne G, Sonnhammer EL (2001) Predicting transmembrane protein topology with a hidden Markov model: application to complete genomes. *J Mol Biol* 305:567–580.
19. Guo H, Bueler SA, Rubinstein JL (2017) Atomic model for the dimeric F_o region of mitochondrial ATP synthase. *Science* 358:936–940.
20. Liu S, et al. (2015) The purification and characterization of ATP synthase complexes from the mitochondria of four fungal species. *Biochem J* 468:167–175.

Results

Fig. S1. Predicted structures of supernumerary subunits of human ATP synthase. (*A-E*), secondary structures of mature subunits e, f-1, g, DAPIT and 6.8PL, respectively, predicted with Jpred 4 (16) and PSIPRED v3.3 (17). H and E below the sequences denote residues predicted to form α-helices or β-sheets, respectively. In subunits e, f-1, DAPIT and 6.8PL, yellow boxed regions are transmembrane α-helices predicted with TMHMM (18). In subunit g, a transmembrane α-helix was predicted by TMpred (https://www.ch.embnet.org/software/TMPRED_form.html), but not TMHMM. In subunits f and g, the N-terminal alanine residues are acetylated, and internal methionine residues, denoted as M, are potential secondary translation initiation sites.

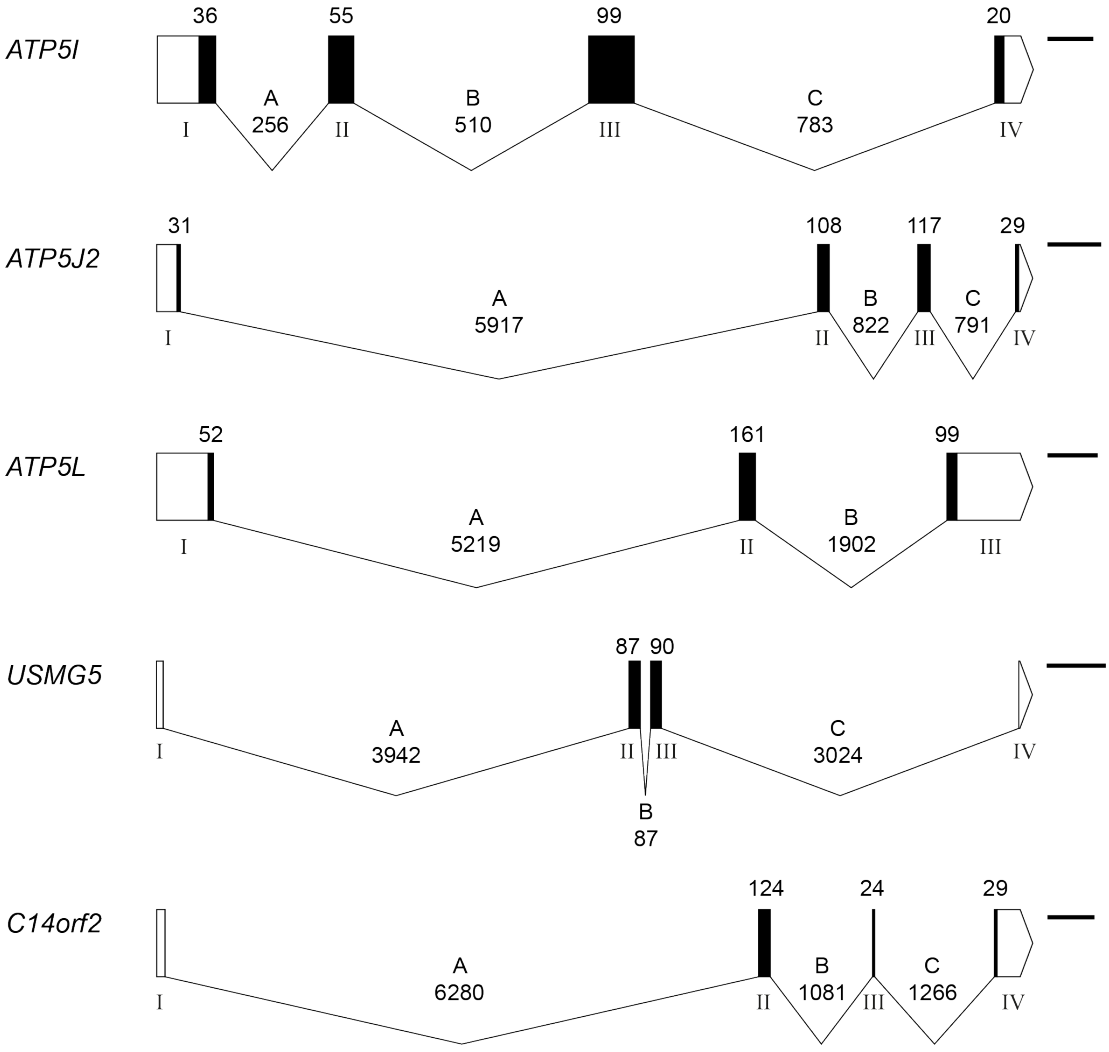

Fig. S2. Structures of the human genes for five supernumerary subunits of ATP synthase. *ATP5I*, *ATP5J2*, *ATP5L*, *USMG5* and *C14orf2* encode the e, f, g, DAPIT and 6.8PL subunits, respectively. Black and unfilled boxes represent, respectively, protein coding and non-coding regions in exons. Exons are labelled with roman numerals. Introns are depicted as intervening continuous lines. The sizes of introns and coding regions of exons are given in base pairs (bp). The scale bar in *ATP5I* represents 100 bp, and those in *ATP5J2*, *ATP5L*, *USMG5* and *C14orf2* correspond to 500 bp. The exon-intron information was obtained from http://www.ensembl.org. The structures of *ATP5I, ATP5J2, ATP5L, USMG5* and *C14orf2* correspond to reference sequences NM_007100, NM_004889, NM_006476, NM_001206426 and NM_004894, respectively. A second isoform of subunit f is produced from an alternative splice variant of *ATP5J2*, at the exon I-intron A boundary, producing a transcript 18 bp shorter at the 3' end of exon I (RefSeq NM_001003713). Images were drawn with the Exon-Intron graphic maker (http://wormweb.org/exonintron).

Table S1. Target sites for gRNA molecules employed in the disruption of human genes *ATP5I, ATP5J2* and *ATP5L*, encoding subunits e, f and g, respectively, of human ATP synthase

gRNA	Sequence
ATP5I-1	GTGCTTCCGGTGCGGAGGTC
ATP5I-2	TCCGCTCATCAAGGTGATCC
ATP5J2-1	TCGCGCGGTCCGGCACAGCG*
ATP5J2-2	GTAAGGCTGTTTGGACTCCG
ATP5L-1	GCGGTTCGGGGCGACGGACT*
ATP5L-2	AGCGCGATGTGAGACCGCCG

*anti-sense sequence used for gRNA

Table S2. Primers employed in the amplification by PCR of regions targeted by gRNAs in *ATP5I*, *ATP5J2* and *ATP5L*.

Primers	Sequence
ATP5I-Forward	CCGCTCTCTCGCCGCT
ATP5I-Reverse	CCAGAGCACTGGGCGG
ATP5J2-Forward	CTGCAGGACCCTCGGATTTT
ATP5J2-Reverse	TTCACCCTCCACGCCTAAC
ATP5L-Forward	GGTTTTCCGGACCTCTACGA
ATP5L-Reverse	ATCTGCAGGTCAGACGAGTG

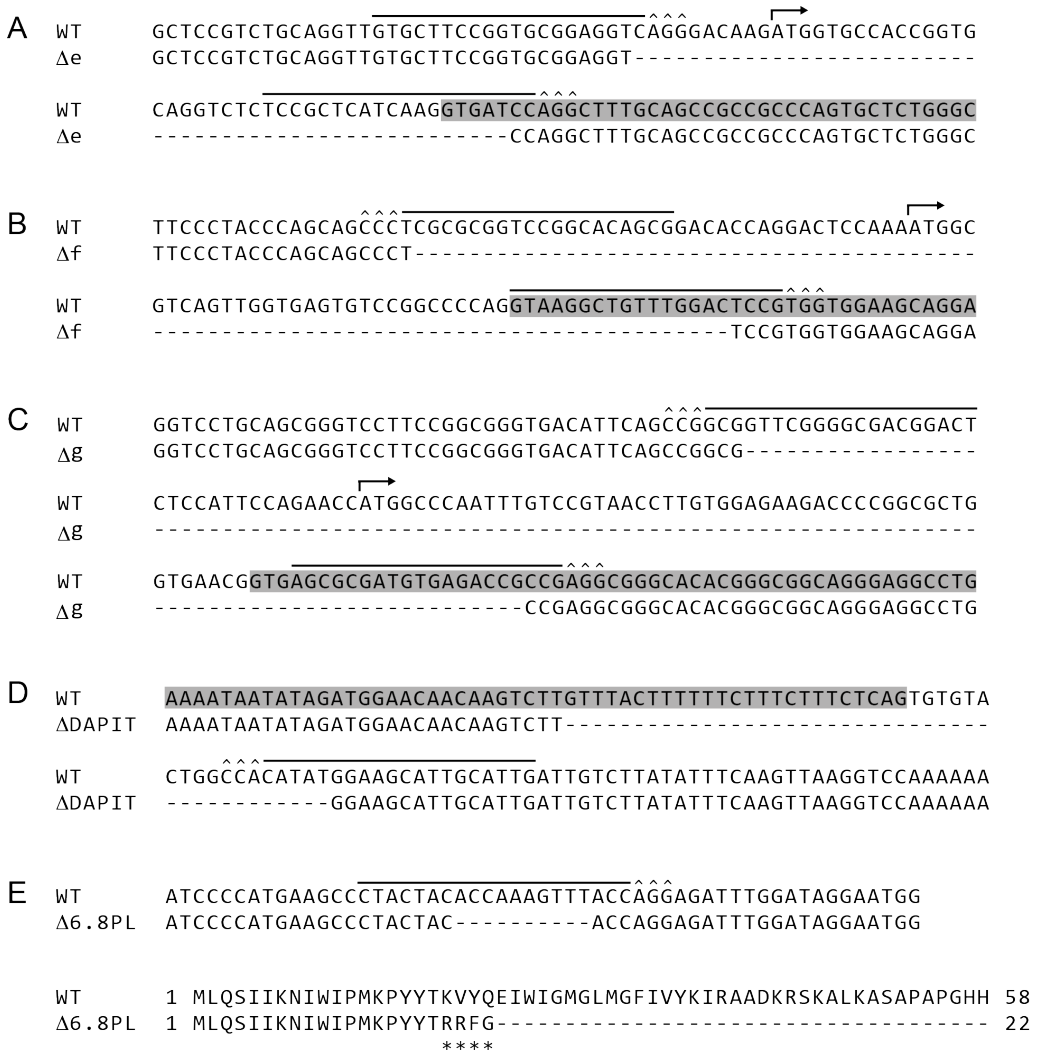

Fig. S3. Disruption of genes for supernumerary subunits of ATP synthase. CRISPR directed deletions were introduced into HAP1 cells in the sequences of the following genes: (*A*), *ATP5I*; (*B*), *ATP5J2*; (*C*), *ATP5L*; (*D*), *USMG5*; and (*E*), *C14orf2*. The corresponding clonal cells HAP1-Δe, -Δf, -Δg, -ΔDAPIT and -Δ6.8PL were isolated subsequently. Carets indicate the PAM (protospacer adjacent motif) sequences for each guide RNA, and solid lines the target sequences for guide RNAs. In (*A*)-(*C*), the wild-type (WT) sequences are parts of exon I and intron A (grey box), aligned with the corresponding deleted sequences. The arrows indicate the start codons in exon I. In (*D*), the WT DNA sequence in part of intron B (grey box) and exon III, is aligned with the corresponding mutated sequence. In (*E*), the upper panel is an internal DNA sequence in exon II of *C14orf2* aligned with the corresponding deleted sequence, and the lower panel shows the impact of the deletion on the sequence of the 6.8PL subunit. In (*A*)-(*E*), the deleted regions are denoted by dashed lines, and in (*E*), asterisks indicate mutations introduced by the process of non-homologous repair.

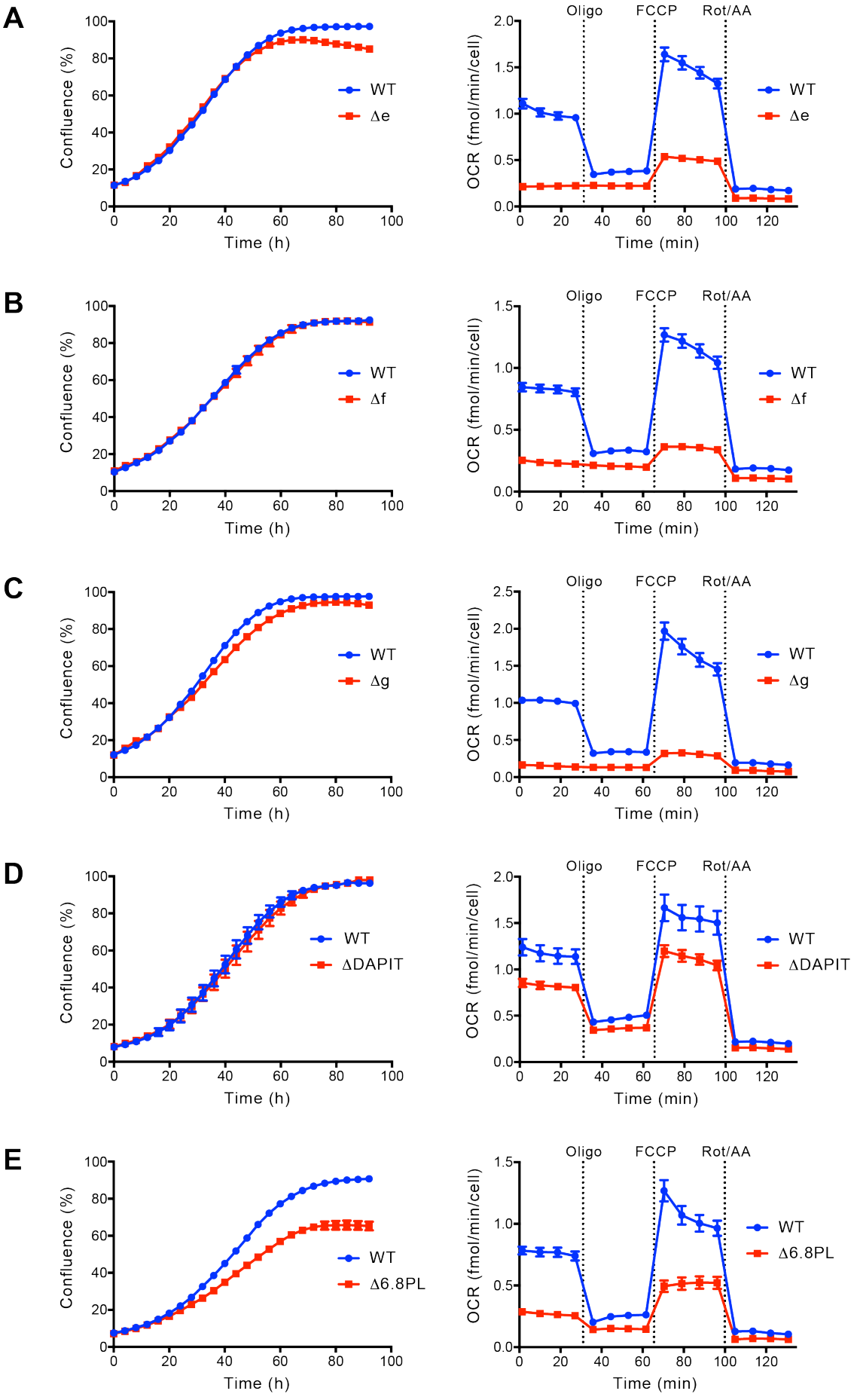
A
Confluence (%)
Time (h)
WT
Δe
Oligo
FCCP
Rot/AA
OCR (fmol/min/cell)
Time (min)
B
Δf
C
Δg
D
ΔDAPIT
E
Δ6.8PL

Fig. S4. Impact of disruption of genes for supernumerary subunits e, f, g, DAPIT and 6.8PL on growth and respiration of HAP1 cells. (*A*-*E*), growth rates (left hand side) and cellular oxygen consumption rates (OCR) (right hand side) of HAP1-WT cells (●) and HAP1 cells with disrupted genes for subunits (■). *A*, Δe; *B*, Δf; *C*, Δg; *D*, ΔDAPIT; *E*, Δ6.8PL. Growth rates were measured by seeding 10^5 cells into each well of a 6-well plate, and by monitoring their confluence over time. Where necessary, initial confluences were adjusted to similar levels for comparison. The data points are the mean values ±SD (n=2-3 wells). OCR was measured before and after sequential additions of oligomycin (Oligo), carbonyl cyanide-4-(trifluoromethoxy)phenylhydrazone (FCCP), and a mixture of rotenone and antimycin A (Rot/AA). Data represent the mean ±SEM (n=6-10 wells).

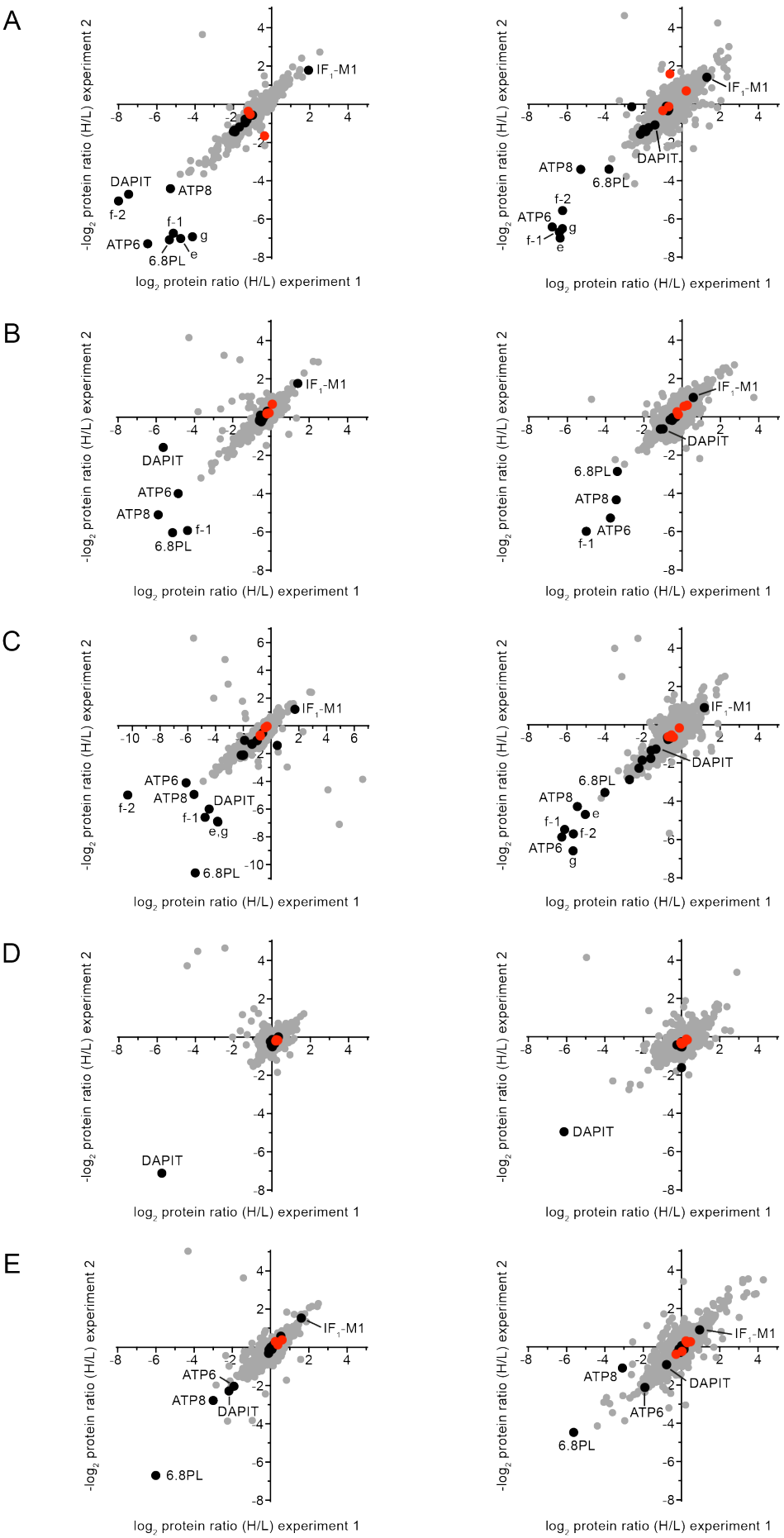
A
B
C
D
E
-log2 protein ratio (H/L) experiment 2
log2 protein ratio (H/L) experiment 1
IF1-M1
DAPIT
ATP8
ATP6
6.8PL
f-1
f-2
g
e
e,g

Fig. S5. Effects on protein relative abundance of the individual deletion of supernumerary subunits of the human ATP synthase complex in HAP1 cells. (*A*)-(*E*), relative abundances of proteins in immuno-purified ATP synthase and vestigial complexes (left-hand panels), and in mitoplasts (right-hand panels). (*A*), HAP1-Δe; (*B*), HAP1-Δf; (*C*), HAP1-Δg; (*D*), HAP1-ΔDAPIT; and (*E*), HAP1-Δ6.8PL. Samples were prepared from a 1:1 mixture of HAP1-Δ cells with HAP1-WT cells that were differentially SILAC-labelled, and the experiments were performed twice, using reciprocal SILAC labelling orientations. The ratios from each experiment are plotted on the horizontal and vertical axes, respectively, of a scatter plot as the log base 2 value. ●, ATP synthase subunits and forms of the inhibitor protein, IF_1; ●, assembly factors ATPAF1, ATPAF2, C7orf55 and TMEM70; ●, all other proteins. Protein ratios are listed in *SI Appendix*, Datasets S1 to S20.

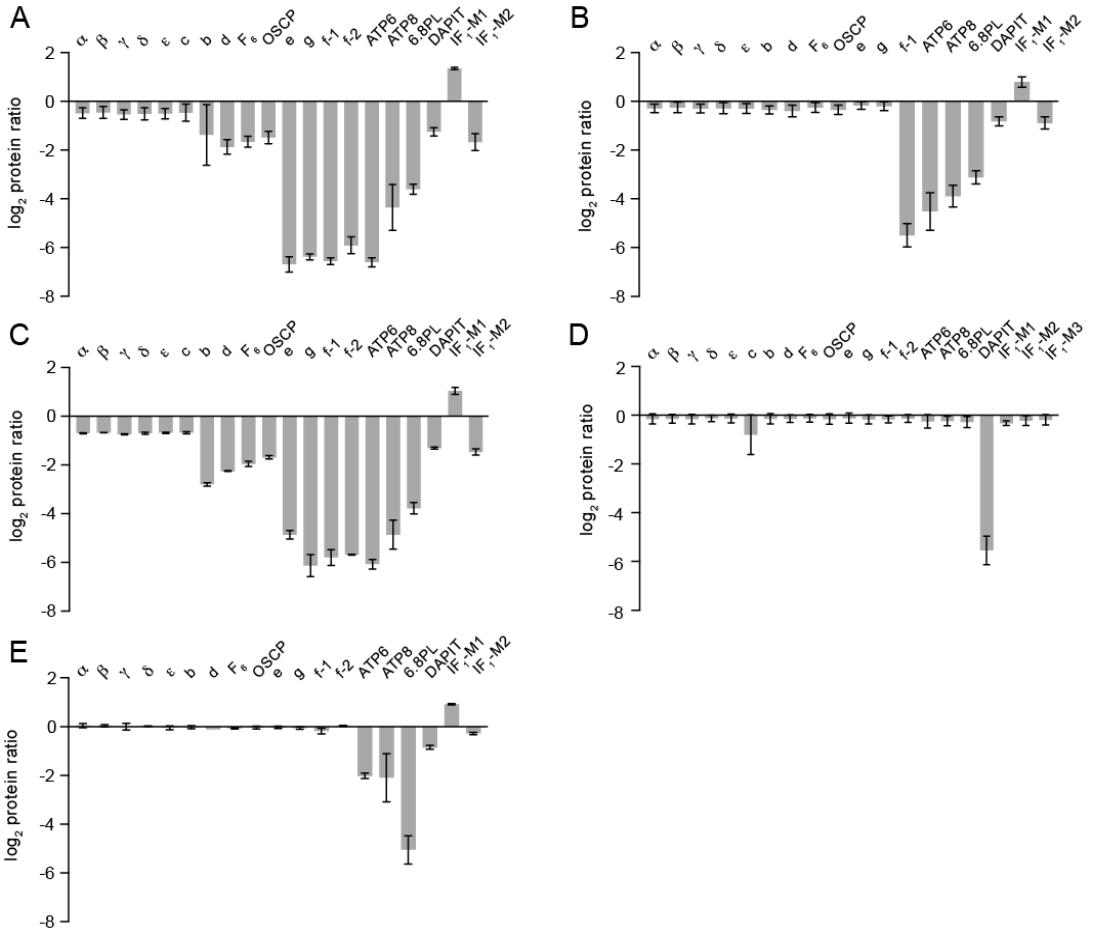

Fig. S6. Effects of removal of individual supernumerary membrane subunits on human ATP synthase. (*A*)-(*E*), relative abundances of ATP synthase subunits, and forms M1, M2 and M3 of IF_1, in mitoplasts from clonal cells. (*A*), HAP1-Δe; (*B*), HAP1-Δf; (*C*), HAP1-Δg; (*D*), HAP1-DAPIT; and (*E*), HAP1-6.8PL. The histograms, derived from *SI Appendix*, Fig. S5 and Datasets S11-S20, are the median values of both relative abundance ratios determined for proteins found in complementary SILAC experiments. Error bars show the range of the two values. IF_1-M1, -M2 and -M3 are different mature forms of IF_1, and f-1 and f-2 are isoforms of subunit f (Swissprot P56134). Except for mitoplasts from HAP1-Δ6.8PL cells, where the values for the 6.8PL and ATP8 are from a single peptide ratio for the control heavy isotope/Δ6.8PL light isotope experiment, the protein ratio is derived from a minimum of two peptide ratios from each complementary SILAC experiment. In the HAP1-Δf and -Δ6.8PL samples, the relative abundance of the c-subunit was not determined.

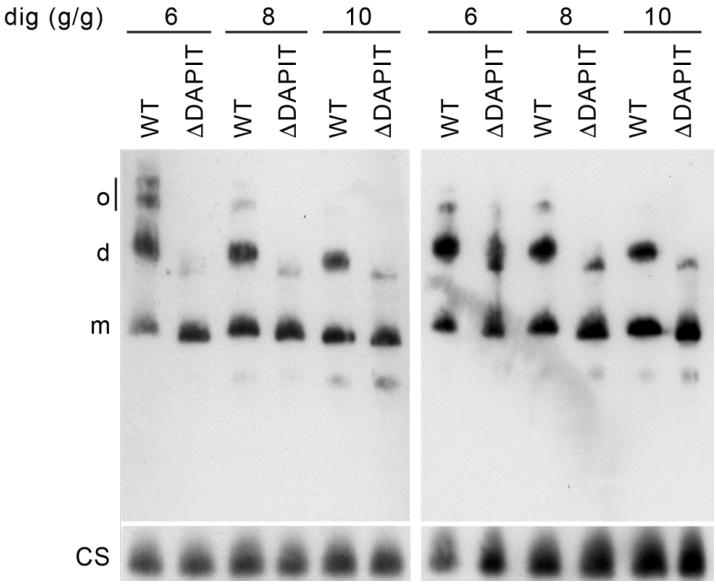

Fig. S7. Effect of deletion of DAPIT on the assembly of ATP synthase. Mitoplasts were prepared from HAP1-wild type cells (WT) and HAP1-ΔDAPIT cells at passage 9 (left hand panels) or passage 24 (right hand panels), solubilized with digitonin (dig), and protein complexes were fractionated by BN-PAGE and transferred electrophoretically to a polyvinylidene difluoride membrane. ATP synthase complexes were detected with an antibody against the α-subunit. o, oligomer; d, dimer; m, monomer. Citrate synthase (CS) was employed as a loading control.

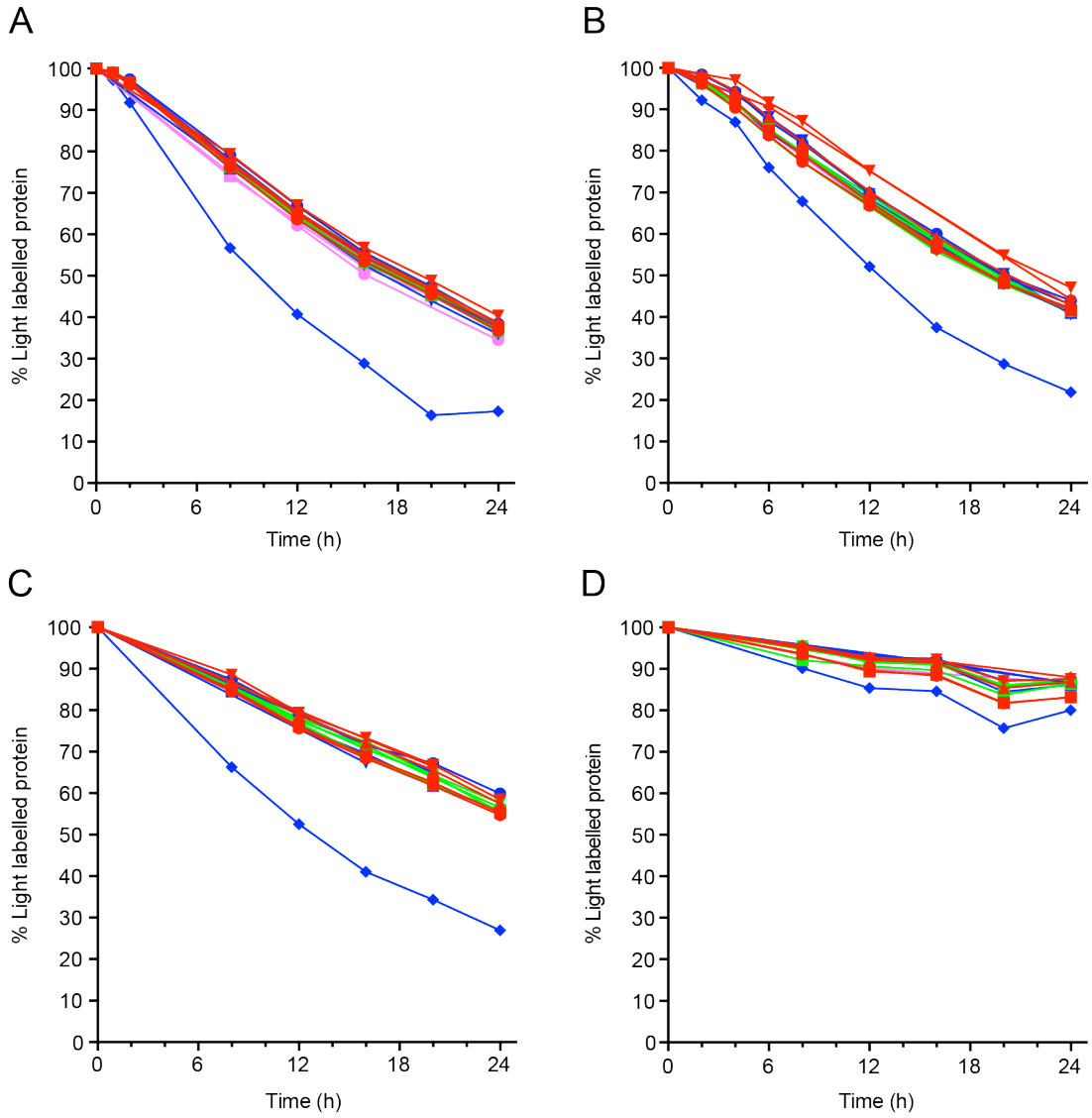

Fig. S8. Turnover of assembled subunits of ATP synthase. Experiments were performed in (*A*), HAP1 cells; (*B*), HEK cells; (*C*) and (*D*), fibroblasts. Cells were grown initially in 'light' SILAC medium and then from time zero in 'heavy' SILAC medium. In (*A*), (*B*) and (*C*), the culture medium contained 25 mM glucose; in (*D*), the glucose was replaced by 25 mM galactose. After various periods of growth, cells were harvested, and mitochondrial membranes were prepared. Membrane proteins were solubilized with DDM (3 g/g), and fractionated by BN-PAGE. The bands containing ATP synthase were excised, the proteins digested with trypsin, and the peptides were analysed by quantitative mass spectrometry. The heavy/light protein ratios produced by MaxQuant were converted to the residual percentage of light-labelled protein. (●), α-subunit; (■), β-subunit; (▲), γ-subunit; (▼), δ-subunit; (◆), ε-subunit; (●), b-subunit; (■), d-subunit; (▲), F_6-subunit; (▼), OSCP; (●), e-subunit;

(■), f-subunit; (▲), g-subunit; (▼), 6.8PL; (◆), DAPIT; (●), ATP6; (■), ATP8. In panel (*A*), no data are shown for the ε-subunit, and in panels (*B*), (*C*) and (*D*), for ATP6. In panel (*C*), single time points represent subunits ε and 6.8PL, and in (*D*), similarly for 6.8PL. The data are taken from *SI Appendix*, Datasets S21 to S24. In (*A*) to (*D*), no data were obtained for subunit c.

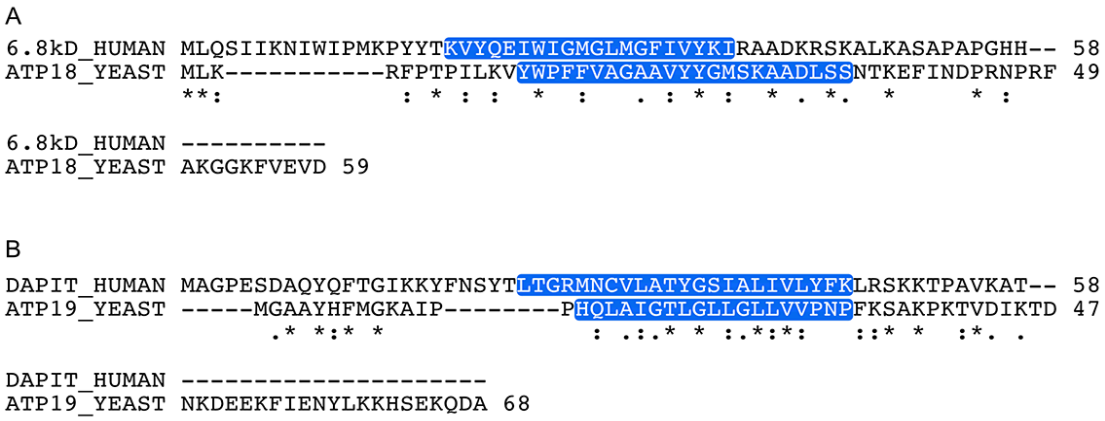

Fig. S9. Comparison of sequences of 6.8PL and DAPIT subunits of human ATP synthase with proposed yeast orthologs. (*A*), 6.8PL and yeast subunit j (ATP18); (*B*), DAPIT and yeast subunit k (ATP19). Asterisks denote identities and colons and full stops conserved residues. The alignments were produced with CLUSTAL. The blue regions denote transmembrane α-helices predicted with Jpred 4 (16) and TMHMM (18) in the human proteins and observed in the structures of the yeast proteins (19).

Table S3. Equivalent genes and orthologous subunits in human and yeast ATP synthases

Human		*S. cerevisiae*	
Gene	Subunit	Gene	Subunit*
ATP5A1	alpha	ATP1	alpha
ATP5B	beta	ATP2	beta
ATP5C1	gamma	ATP3	gamma
ATP5D	delta	ATP16	delta
ATP5E	epsilon	ATP15	epsilon
ATP5F1	F_o complex B1 or b	ATP4	4 or b
ATP5G1	F_o complex C1†	ATP9 or OLI1	9 or c
ATP5G2	F_o complex C2†	-	-
ATP5G3	F_o complex C3†	-	-
ATP5H	d	ATP7	d
ATP5I	e	ATP21 or TIM11	e
ATP5J	coupling factor 6 or F_6	ATP14	h
ATP5J2	f	ATP17	f
ATP5L	g	ATP20	g
ATP5O	O or OSCP	ATP5	5 or OSCP
MT-ATP6	a or ATP6	ATP6	a or ATP6
MT-ATP8	protein 8, ATP8 or A6L	ATP8	8 or Aap1
C14orf2	6.8 kDa mitochondrial proteolipid	ATP18	i or j
USMG5	Diabetes-associated protein in insulin-sensitive tissues	ATP19	k

* Subunit l (20) was not found in the structure of F_o from *S. cerevisiae* (19).

† C1, C2 and C3 are identical subunits encoded in three different genes.

Table S4. Sources of Antibodies

Protein	Source	Antibody
ATP synthase α	Proteintech	14676-1-AP
ATP synthase γ	Sigma	SAB2700096
ATP synthase e	Sigma	HPA035010
ATP synthase f	Santa Cruz Biotechnology	sc-241862
ATP synthase DAPIT	Proteintech	17716-1-AP
ATP synthase 6.8PL	Sigma	HPA058978